Physics and Chemistry of Minerals (2019) 46:157–163
https://doi.org/10.1007/s00269-018-0994-6

ORIGINAL PAPER

Crystal chemistry of Eu-bearing tuite synthesized at high-pressure and high-temperature conditions

Shuangmeng Zhai[1] · Hexiong Yang[2] · Weihong Xue[1] · Eugene Huang[3] · Daisuke Yamazaki[4] · Shaunna M. Morrison[2,5] · Robert T. Downs[2]

Received: 1 May 2018 / Accepted: 22 July 2018 / Published online: 27 July 2018

Abstract
Tuite, γ-$Ca_3(PO_4)_2$, is a potential host for rare-earth elements in the deep mantle. Eu-bearing tuite single crystals with chemical formulas of $Ca_{2.93}Eu_{0.04}(PO_4)_2$ and $Ca_{2.88}Eu_{0.07}Na_{0.06}(PO_4)_2$ were synthesized at 16 GPa and 1600 °C, and their structures were investigated at room temperature with single-crystal X-ray diffraction. The structure refinements of Eu-bearing tuite indicate the preference of Eu^{3+} for the smaller 6-coordinated Ca1 site with a coupled vacancy due to the substitution of $2Eu^{3+} + \square \rightarrow 3\ Ca^{2+}$. In NaEu-bearing tuite, both Eu^{3+} and Na^{+} occupy the smaller 6-coordinated Ca1 site according to the coupled substitution of $Eu^{3+} + Na^{+} \rightarrow 2\ Ca^{2+}$. The presence of Na results in more Eu_2O_3 in NaEu-bearing tuite, because the coupled substitution is energetically more favorable. REE-bearing tuite could be found on the Moon and the deep Earth's mantle as a consequence of REE-bearing apatite or/and merrillite transformation under high-pressure and high-temperature conditions.

Keywords Eu-bearing · Tuite · γ-$Ca_3(PO_4)_2$ · Crystal structure · Single-crystal X-ray diffraction

Introduction

Apatite is a common accessory mineral occurring in a variety of terrestrial rocks, as well as lunar rocks and meteorites (Nash 1984). It is a primary host for rare-earth elements (REE) and large ion lithophile elements (such as U, Th, Ba, and Sr) in lunar rocks and the Earth's mantle (Griffin et al. 1972; Puchelt and Emmermann 1976; Beswick and Carmichael 1978; Jolliff et al. 1993). Under upper mantle conditions, apatites decompose to form γ-$Ca_3(PO_4)_2$ (Murayama et al. 1986). The γ-$Ca_3(PO_4)_2$ phase is also one of the decomposed products of merrillite under high-pressure and high-temperature conditions (Zhai et al. unpublished results). The natural occurrence of γ-$Ca_3(PO_4)_2$, first found in the Suizhou L6 chondrite, was described and named tuite (Xie et al. 2002, 2003). Tuite was subsequently found in other meteorites (Miyahara et al. 2009; Baziotis et al. 2013; Boonsue and Spray 2012; Hu and Sharp 2016; Litasov and Podgornykh 2017). Natural tuite can also be formed from chlorapatite after its decomposition under pressure (Xie et al. 2013). A previous study shows that tuite may be stable under the lower mantle conditions (Zhai et al. 2013). It is known that merrillite can accommodate a significant amount of REE (up to 13 wt%) (Jolliff et al. 1993, 2006). Therefore, tuite, as a main run product of apatite and merrillite under high-pressure and high-temperature conditions, is potentially a host for REE in the deep upper mantle (Murayama et al. 1986; Sugiyama and Tokonami 1987; Xie et al. 2003; Zhai et al. 2013; Skelton and Walker 2017).

Electronic supplementary material The online version of this article (https://doi.org/10.1007/s00269-018-0994-6) contains supplementary material, which is available to authorized users.

✉ Shuangmeng Zhai
zhaishuangmeng@vip.gyig.ac.cn

[1] Key Laboratory of High-temperature and High-pressure Study of the Earth's Interior, Institute of Geochemistry, Chinese Academy of Sciences, Guiyang 550081, Guizhou, China

[2] Department of Geosciences, University of Arizona, Tucson, AZ 85721-0077, USA

[3] Center for High Pressure Science and Technology Advanced Research, Shanghai 201203, China

[4] Institute for Planetary Materials, Okayama University, Misasa, Tottori 682-0193, Japan

[5] Geophysical Laboratory, Carnegie Institution for Science, Washington, DC 20015, USA

Partitioning studies on ten trace elements (including Nb, Ta, Zr, Y, Ba, Sr, Rb, Ce, Nd, and Lu) in apatite–silicate systems under high-pressure and high-temperature conditions showed that tuite can contain REE (Konzett and Frost 2009; Konzett et al. 2012). Eu^{3+}- and Sm^{3+}-doped tuites were synthesized at high-pressure and high-temperature conditions and their photoluminescences were investigated (Xue et al. 2012, 2015). Large REE-bearing tuite crystals were synthesized at 15 GPa and 1800 K using a natural apatite sample as starting material, and it was found that the concentrations of REE in tuite are 2–3 orders higher than those in upper mantle silicate minerals, such as garnet and diopside (Zhai et al. 2014).

The crystal structure of tuite has been reported (Sugiyama and Tokonami 1987; Thompson et al. 2013). However, there is no detailed information for the crystal chemistry of rare-earth elements in tuite. In the present study, Eu-bearing tuite single crystals with chemical formulas of $(Ca_{2.93}Eu_{0.04})(PO_4)_2$ and $(Ca_{2.88}Eu_{0.07}Na_{0.06})(PO_4)_2$ were synthesized at 16 GPa and 1600 °C using mixtures of hydroxyapatite, Eu_2O_3 and NaF as starting materials. The crystal structure was determined by single-crystal X-ray diffraction.

Experimental

High-purity reagents of $Ca_5(PO_4)_3OH$, Eu_2O_3, and NaF were used to prepare starting materials for high-pressure and high-temperature experiments. A mixture of $Ca_5(PO_4)_3OH$ plus 5 wt% Eu_2O_3 was prepared as the starting material for the Eu-bearing tuite, while a mixture containing $Ca_5(PO_4)_3OH$, NaF and Eu_2O_3 in a molar ratio of 1:0.15:0.075 was used for the Na–Eu-bearing tuite. High-pressure and high-temperature experiments were performed using a kawai-type multi-anvil high-pressure apparatus, USSA-5000, at the Institute for Planetary Materials, Okayama University (Misasa, Japan). The experimental method is similar to that described in Xue et al. (2009). The sample assembly is shown in Fig. 1. Samples were compressed by eight cubic tungsten carbide anvils of 32 mm edge length and 6 mm truncation edge length. Pyrophyllite was adopted as a gasketing material. A Cr-doped MgO octahedron of 14 mm edge length was used as the pressure medium. A stepped $LaCrO_3$ cylindrical heater was embedded in a ZrO_2 thermal isolating sleeve. The starting material was put into a Pt capsule (2.5 mm OD, ca. 2.5 mm length) placed near the center of the heater and surrounded by MgO sleeve. A $W_{97}Re_3$–$W_{75}Re_{25}$ thermocouple was used for temperature measurement. After each sample was kept at 16 GPa and 1600 °C for 15 h, it was then cooled to room temperature within 2 min and then slowly decompressed to ambient pressure.

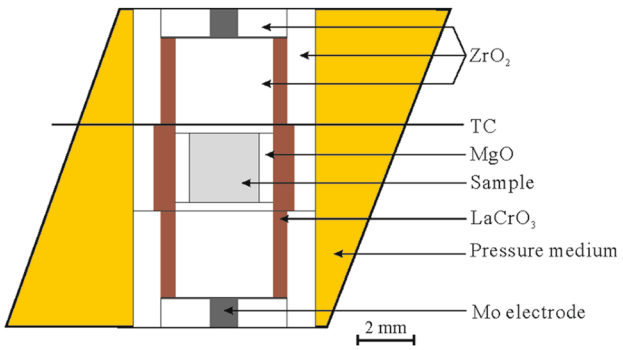

Fig. 1 Schematic drawings of the sample assembly

According to the phase diagram, the decomposed products of hydroxyapatite at 16 GPa and 1600 °C include tuite and $Ca(OH)_2$ or CaO plus H_2O (Murayama et al. 1986). Preliminary identification of tuite in the products was performed using a micro-focused X-ray diffractometer (RINT RAPID II-CMF) equipped with a rotating Cu anode operated at 40 kV and 30 mA. A scanning electron microprobe (JSM-7001F) was used to examine the synthesized crystals and images are shown in Fig. 2. Besides tuite, it is clear that there is a minor phase with Ca- and Eu enrichments in the run products, since some Eu_2O_3 was added, shown as bright parts in Fig. 2a. SEM mapping analysis indicates that the Eu-bearing tuite crystals are chemically homogeneous.

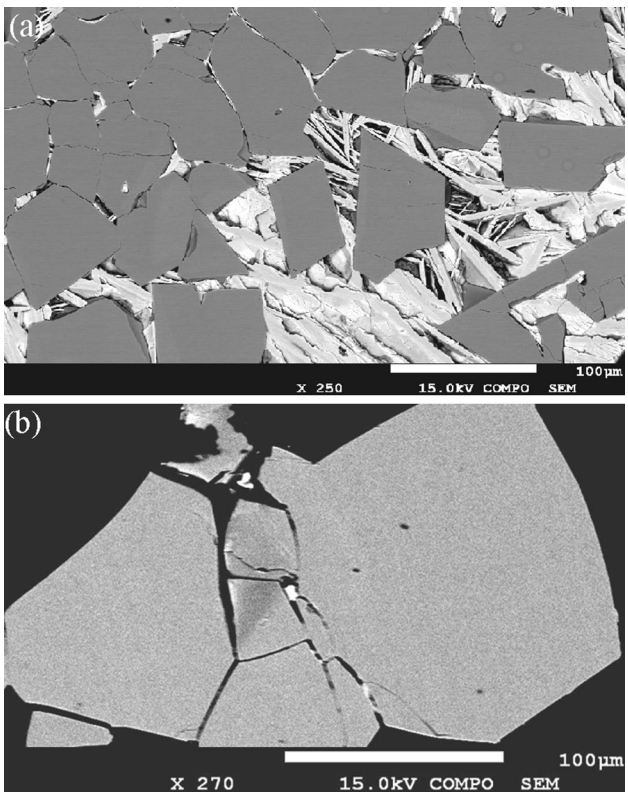

Fig. 2 SEM images of the Eu-bearing tuite (**a**) and NaEu-bearing tuite (**b**) crystals

Chemical compositions of the tuite crystals were determined by an electron probe microanalyzer (JXA-8800) operated at 15 kV and 12 nA. The average compositions (wt%) for 12 analyzed points are CaO 52.33(5), Eu_2O_3 2.24(2), P_2O_5 45.21(10), with total = 99.78(9), giving an empirical chemical formula (based on 8 O apfu) $Ca_{2.93}Eu_{0.04}(PO_4)_2$ for Eu-bearing tuite (Eu–Tu), and CaO 50.82(9), Eu_2O_3 3.64(7), Na_2O 0.60(2), P_2O_5 44.61(16), with total = 99.68(17), yielding an empirical chemical formula (based on 8 O apfu) $Ca_{2.88}Eu_{0.07}Na_{0.06}(PO_4)_2$ for Na and Eu-bearing tuite (NaEu–Tu).

Single-crystal X-ray diffraction data for both Eu–Tu and NaEu–Tu were collected from nearly equi-dimensional crystals on a Bruker X8 APEX2 CCD X-ray diffractometer equipped with graphite-monochromatized MoKα radiation with frame widths of 0.5° in ω and 30 s counting time per frame. All reflections were indexed on the basis of a trigonal unit cell (Table 1). The intensity data were corrected for X-ray absorption using the Bruker program SADABS. The crystal structure was refined using SHELX2014 (Sheldrick 2015a, b) based on space group *R-3m* and the model of Thompson et al. (2013). The positions of all atoms were refined with full occupancies and anisotropic displacement parameters, except for the Ca1 site of Eu-bearing tuite, which was constrained to (0.94 Ca + 0.04 Eu + 0.02 □). Table 1 summarizes the details on data collection and structure refinement. Table 2 gives the fractional atomic coordinates, occupancy, site symmetry, and equivalent atomic displacement parameters (U_{eq}). Table 3 lists the anisotropic atomic displacement parameters (U_{ij}). Table 4 presents selected interatomic distances. The crystal structures of both Eu–Tu and NaEu–Tu have been formatted into CIF files, which are attached as supplementary material.

Raman spectra of the samples were measured with a Thermo-Almega microRaman system. A solid-state laser with a wavelength of 780 nm was used as excitation source and the signal was processed by a thermoelectrically cooled CCD detector. The laser is partially polarized with 4 cm^{-1} resolution and focused to a spot size of 1 μm on the sample. The laser power was 200 mW and each spectrum was the sum of 12 scans of 30 s accumulation time.

Results and discussion

The crystal structures of Eu–Tu and NaEu–Tu are comparable with the pure tuite synthesized from $Ca_5(PO_4)_3Cl$ at 15 GPa and 1300 °C (Thompson et al. 2013). In tuite, the Ca cations occupy two symmetrically nonequivalent sites, Ca1 (equipoint 3*a*, CaO_{12} polyhedron) and Ca2 (equipoint 6*c*, CaO_{10} polyhedron). The Ca1 site displays a (6 + 6) coordination, with six Ca1–O-bond lengths (2.4404 Å) markedly

Table 1 Summary of crystal data and refinement results

	Eu–Tu	NaEu–Tu	Tu
Ideal chemical formula	$Ca_3(PO_4)_2$	$Ca_3(PO_4)_2$	$Ca_3(PO_4)_2$
Empirical chemical formula	$(Ca_{2.93}Eu_{0.04})(PO_4)_2$	$(Ca_{2.88}Eu_{0.07}Na_{0.06})(PO_4)_2$	$Ca_{2.98}(P_{1.01}O_4)_2$
Structural formula	$(Ca_{2.94}Eu_{0.04}□_{0.02})(PO_4)_2$	$(Ca_{2.88}Eu_{0.06}Na_{0.06})(PO_4)_2$	$Ca_3(PO_4)_2$
Crystal size (mm)	0.07 × 0.07 × 0.06	0.06 × 0.05 × 0.05	0.05 × 0.05 × 0.04
Space group	*R*-3*m*	*R*-3*m*	*R*-3*m*
a (Å)	5.2531(3)	5.2519(4)	5.2522(9)
c (Å)	18.6858(9)	18.6885(2)	18.690(3)
V (Å^3)	446.55(4)	446.41(6)	446.5(2)
Z	3	3	3
ρ_{cal} (g/cm^3)	3.501	3.525	3.461
λ (Å, Mo*Kα*)	0.71069	0.71069	0.71073
μ (mm^{-1})	3.70	3.848	3.33
$2\theta_{MAX}$ for data collection	≤65.16	≤65.16	≤66.08
No. of reflections collected	1399	1465	1495
No. of independent reflections	235	235	243
No. of reflections with $I > 2\sigma(I)$	222	222	216
No. of parameters refined	21	21	19
R (int)	0.022	0.018	0.016
Final R_1, wR_2 factors [$I > 2\sigma(I)$]	0.021, 0.058	0.021, 0.059	0.018, 0.051
Final R_1, wR_2 factors (all data)	0.022, 0.062	0.022, 0.060	0.021, 0.053
Goodness-of-fit	1.178	1.148	1.080
Reference	This study	This study	Thompson et al. (2013)

Table 2 Atoms, Wyckoff positions, site occupation factors (sof), fractional atomic coordinates, and equivalent isotropic displacement parameters for tuites

Atom	Wyckoff	sof	*x*	*y*	*z*	U_{iso}
Eu–Tu						
Ca1	3*a*	0.94	0	0	0	0.0149(2)
Eu1	3*a*	0.04	0	0	0	0.0149(2)
Ca2	6*c*		0	0	0.20353(2)	0.0102(2)
P	6*c*		0	0	0.40497(3)	0.0060(2)
O1	6*c*		0	0	0.32366(9)	0.0166(4)
O2	18*h*		0.1736(1)	0.3472(2)	0.09938(5)	0.0115(3)
EuNa–Tu						
Ca1	3*a*	0.88	0	0	0	0.0143(2)
Eu1	3*a*	0.06	0	0	0	0.0143(2)
Na1	3*a*	0.06	0	0	0	0.0143(2)
Ca2	6*c*		0	0	0.20346(2)	0.0113(2)
P	6*c*		0	0	0.40496(3)	0.0066(2)
O1	6*c*		0	0	0.32372(9)	0.0176(4)
O2	18*h*		0.1736(1)	0.3472(2)	0.09934(5)	0.0120(3)
Tu[a]						
Ca1	3*a*		0	0	0	0.0128(2)
Ca2	6*c*		0	0	0.20359(2)	0.0100(2)
P	6*c*		0	0	0.40508(3)	0.0060(2)
O1	6*c*		0	0	0.32372(8)	0.0151(4)
O2	18*h*		0.1737(1)	0.3474(2)	0.09950(4)	0.0114(2)

[a]Data from Thompson et al. (2013)

Table 3 Anisotropic displacement parameters U_{ij} ($Å^2$) for tuites

Atom	U_{11}	U_{22}	U_{33}	U_{12}	U_{13}	U_{23}
Eu–Tu						
M1	0.0178(3)	0.0178(3)	0.0060(3)	0.0089(2)	0	0
M2	0.0119(3)	0.0119(3)	0.0067(3)	0.0060(1)	0	0
P	0.0062(3)	0.0062(3)	0.0055(3)	0.0031(1)	0	0
O1	0.0214(6)	0.0214(6)	0.0069(7)	0.0107(3)	0	0
O2	0.0141(4)	0.0068(5)	0.0110(4)	0.0034(2)	0.0002(2)	0.0003(3)
EuNa–Tu						
M1	0.0185(3)	0.0185(3)	0.0060(3)	0.0093(1)	0	0
M2	0.0132(3)	0.0132(3)	0.0076(3)	0.0066(1)	0	0
P	0.0069(3)	0.0069(3)	0.0059(3)	0.0035(1)	0	0
O1	0.0227(6)	0.0227(6)	0.0075(7)	0.0114(3)	0	0
O2	0.0149(4)	0.0074(5)	0.0113(5)	0.0037(2)	0.0002(2)	0.0004(3)
Tu[a]						
M1	0.0163(3)	0.0163(3)	0.0058(3)	0.0082(1)	0	0
M2	0.0116(2)	0.0116(2)	0.0069(2)	0.0058(1)	0	0
P	0.0064(2)	0.0064(2)	0.0052(3)	0.0032(1)	0	0
O1	0.0193(6)	0.0193(6)	0.0066(7)	0.0097(3)	0	0
O2	0.0139(4)	0.0073(4)	0.0106(4)	0.0036(2)	0.0002(1)	0.0005(3)

The M1 site contains (0.94 Ca + 0.04 Eu + 0.02 □) for Eu–Tu and (0.88 Ca + 0.06 Eu + 0.06 Na) for NaEu–Tu. The M2 site is fully filled with Ca for both Eu–Tu and NaEu–Tu samples

[a]Data from Thompson et al. (2013)

Table 4 Selected bond lengths (Å) determined by single-crystal XRD

		Eu–Tu	EuNa–Tu	Tu[a]
M1–O1	×6	3.0382(2)	3.0375(3)	3.0377(5)
M1–O2	×6	2.4378(8)	2.4374(9)	2.4404(9)
Avg.		2.7380	2.7375	2.739
M2–O1		2.245(2)	2.248(2)	2.245(2)
M2–O2	×3	2.5064(9)	2.506(1)	2.507(1)
M2–O2	×6	2.6881(2)	2.6880(3)	2.6870(5)
Avg.		2.589	2.589	2.589
P–O1		1.519(2)	1.518(2)	1.521(2)
P–O2	×3	1.543(1)	1.542(1)	1.542(1)
Avg.		1.537	1.536	1.537

The M1 site contains (0.94 Ca + 0.04 Eu + 0.02 □) for Eu–Tu and (0.88 Ca + 0.06 Eu + 0.06 Na) for NaEu–Tu. The M2 site is fully filled with Ca for both Eu–Tu and NaEu–Tu samples

[a]Data from Thompson et al. (2013)

shorter than the other six Ca1–O bonds (3.0377 Å), whereas the Ca2 site is 10-coordinated with an average Ca2–O bond of 2.589 Å (Thompson et al. 2013). Our structure refinements indicate that Eu prefers the Ca1 site in tuite. As listed in Table 4, the average P–O, Ca2–O, and longer Ca1–O-bond lengths are similar for Tu, Eu–Tu, and NaEu–Tu samples, but the shorter Ca1–O-bond lengths are slight different for the three samples.

The major structural difference between the pure tuite and Eu-bearing tuites is that some Ca is substituted according to the mechanisms of $2\,Eu^{3+} + \square \rightarrow 3\,Ca^{2+}$ in Eu–Tu and $Eu^{3+} + Na^{+} \rightarrow 2\,Ca^{2+}$ in NaEu–Tu. The previous studies have showed that such coupled substitution mechanisms are common in apatites (Hughes and Cameron 1991; Fleet and Pan 1994, 1995; Pan and Fleet 2002). Compared to the coupled vacancy substitution of $2\,Eu^{3+} + \square \rightarrow 3\,Ca^{2+}$, the coupled substitution of $Eu^{3+} + Na^{+} \rightarrow 2\,Ca^{2+}$ should be energetically more favorable, resulting in more Eu_2O_3 in NaEu–Tu (0.04 apfu in Eu–Tu vs. 0.06 apfu in NaEu–Tu).

The Raman spectra of natural and synthetic tuite were reported in the previous studies (Xie et al. 2003, 2013, 2016; Zhai et al. 2010a, b, 2011, 2014; Hu and Sharp 2016; Litasov and Podgornykh 2017). Figure 3 displays the synthetic Eu-bearing tuites. For comparison, the Raman spectrum of a pure tuite synthesized in Thompson et al. (2013) is also collected and is shown in Fig. 3. There is no obvious difference among these samples in the range of 400–1100 cm^{-1} primarily attributed to the internal PO_4 vibrational modes, which is consistent with the single-crystal X-ray refinements that indicates the PO_4 tetrahedra (including the P–O-bond length, O–P–O angle) in these three samples are nearly identical. Nonetheless, some difference occurs in the low Raman shift region less than 350 cm^{-1} that corresponds to the external modes

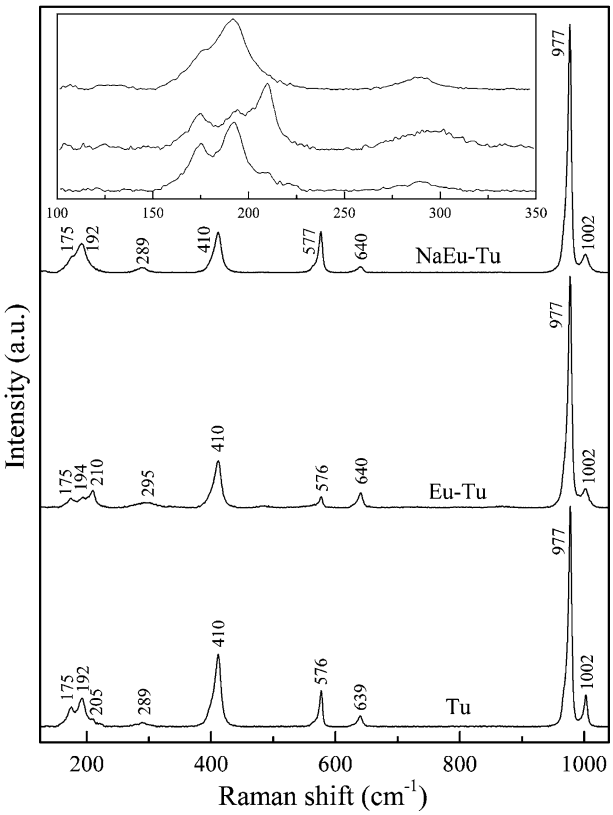

Fig. 3 Raman spectra of synthetic tuite crystals. The insert plot shows the enlarged Raman spectra between 100 and 350 cm^{-1}

involving Ca translations, which is clear shown in the insert of Fig. 3. The relative intensities and wavenumbers of external modes are different for the three samples. In the lower wavenumber region (less than 350 cm^{-1}), the 209 cm^{-1} band is most strongest for the Eu–Tu sample, but the 192 cm^{-1} band is the most strongest for Tu and NaEu–Tu samples. This is reasonable as Ca is partially substituted by Eu or Eu + Na in Eu-bearing tuite, causing the changes of Raman shift and intensity of bands, where cationic translations are involved.

Tuite has only been found in shocked meteorites thus far. There is no information about the REE concentration and their crystal chemistry in natural tuite. The present synthetic Eu-bearing tuite crystals contain 2.2 and 3.6 wt% Eu_2O_3 in Eu–Tu and NaEu–Tu, respectively. It means that the presence of Na can enhance the content of Eu_2O_3 accommodated in tuite, though tuite formed from apatite in meteorites contains no or less than 0.25% of Na_2O (Xie et al. 2013). On the other hand, natural tuite formed from merrillite in meteorites has been found to contain Na_2O up to about 2.86 wt% (Xie et al. 2002, 2003; Litasov and Podgornykh 2017). In addition, Na in merrillite has its own occupation site in the structural complexes of $[Ca_9Na(PO_4)]^{16+}$ and plays a critical role in maintaining the charge balance (Xie et al. 2015). Therefore, the accommodated

amount of REE in these two kinds of natural tuite might be different.

Though no information about the accommodation of REE in tuite formed from merrillite is available, a few previous studies show that tuite formed from apatite can contain some amount of REE. By doping with 250–350 ppm trace elements including Ce, Nd, Lu, and Y in apatite–MORB and apatite–peridotite systems, Konzett and Frost (2009) and Konzett et al. (2012) checked the concentrations of Ce and Nd in tuite by EPMA and found that tuite has distinctly higher Ce and Nd (up to 4.27 wt% Ce_2O_3 and 3.55 wt% Nd_2O_3) which is related to the content of Na. Eu- and Sm-doped tuite samples (with 3.0 wt% Eu_2O_3 and 1.1 wt% Sm_2O_3) were also synthesized (Xue et al. 2012, 2015). Zhai et al. (2014) used a natural REE-bearing apatite to obtain some large tuite crystals and analyzed the concentrations of REE by LA–ICP–MS. The results showed that REE contents are from a few ppm to 2.5 wt%.

As a run product of apatite (Murayama et al. 1986) and merrillite (Zhai et al. unpublished results) under high-pressure and high-temperature conditions, REE-bearing tuite could be found on the Moon as a consequence of REE-bearing apatite or/and merrillite transformation under impacts. It is known that apatite and merrillite were found as minor phases in lunar rocks from Apollo samples (Griffin et al. 1972; Dickinson and Hess 1983). The lunar surface has been undergone periods of intense meteorite bombardment over geologic time (Stöffler et al. 2006). Therefore, some tuite may form after apatite and/or merrillite subjected to meteorite bombardment with enough high pressure and temperature for the transformations. Moreover, REE-bearing apatite may be transported into the deep mantle and decompose into REE-bearing tuite under the high-pressure and high-temperature conditions. Indeed, Murayama et al. (1986) showed that at 11–13 GPa between 1000 and 1500 °C pure hydroxyapatite and fluorapatite decompose with a negative slope of the apatite–tuite phase boundary in a following reaction:

$$2\ \text{apatite} \rightarrow 3\ \text{tuite} + \text{X},$$

where X may be $Ca(OH)_2$, $CaO + H_2O$, or $CaO + H_2O(\uparrow)$ for OH apatite and CaF_2 for F apatite. Konzett and Frost (2009) experimentally showed that in an average MORB and a model Mg-basalt systems, hydroxyapatite transforms to tuite at pressure above 7.5 GPa and temperature of 950 °C by reactions involving garnet and SiO_2, which is ~ 5 GPa lower than the stability limit of pure OH–apatite. As proposed by Konzett and Frost (2009), the possible tuite-forming reactions are as follows:

$$12\ \text{apatite} + \text{pyrope} + 6\ \text{coesite} \rightarrow 18\ \text{tuite} + \text{grossular} + 3\ \text{diopside} + 6\ H_2O,$$

$$12\ \text{apatite} + 2\ \text{pyrope} + 6\ \text{coesite} \rightarrow 18\ \text{tuite} + 2\ \text{grossular} + 3\ \text{enstatite} + 6\ H_2O,$$

$$4\ \text{apatite} + \text{enstatite} + 2\ \text{coesite} \rightarrow 6\ \text{tuite} + 2\ \text{diopside} + 2\ H_2O.$$

In peridotite–apatite system, apatite is stable to at least 8.7 GPa at 1000 °C, which is about ~ 1 GPa above the stability limit of apatite within a MORB composition, and the possible tuite-forming reactions are as follows (Konzett et al. 2012):

$$2\ \text{apatite} + 3\ \text{enstatite} \rightarrow 3\ \text{tuite} + \text{forsterite} + \text{diopside} + H_2O,$$

$$4\ \text{apatite} + \text{pyrope} + \text{diopside} \rightarrow 6\ \text{tuite} + \text{grossular} + 2\ \text{forsterite} + H_2O,$$

$$6\ \text{apatite} + \text{pyrope} + 3\ \text{enstatite} \rightarrow 9\ \text{tuite} + \text{grossular} + 3\ \text{forsterite} + 2\ H_2O.$$

The mean Ca–O-bond lengths of two kinds of 12 and 10 coordinated Ca in tuite are longer than those of different coordinated Ca in apatite and in mantle silicates (e.g., garnet and diopside). In apatite–MORB and apatite–peridotite systems, the concentrations of Ce_2O_3 and Nd_2O_3 in tuite are higher than those in apatite (Konzett and Frost 2009; Konzett et al. 2012). However, the concentrations of REE in tuite synthesized at 15 GPa and 1800 K using a natural REE-bearing apatite as starting material are slightly lower than those in apatite (Zhai et al. 2014). Compared with those in natural garnets and pyroxenes (Zheng et al. 2005; Python et al. 2007; Gaspar et al. 2008; Zhang et al. 2009; Dégi et al. 2010; Santosh et al. 2010), the concentrations of REE in tuite are 2–3 order higher (Zhai et al. 2014). Therefore, REE in tuite has important geochemical implications.

Acknowledgements We thank Prof. Taku Tsuchiya for his editorial handling. Critical comments and suggestion from Prof. Xiande Xie and an anonymous reviewer are helpful to improve the manuscript. This work was financially supported by the National Natural Science Foundation of China (Grant no. 41372040), Western Light Talents Training Program of CAS, Science and Technology Department of Guizhou Province (Grant nos. [2015] 2140 and [2016] 1157), Science Foundation Arizona, and Visiting Researcher's Program of the Institute for Planetary Materials, Okayama University.

References

Baziotis IP, Liu Y, DeCarli PS, Melosh HJ, McSween HY, Bodnar RJ, Taylor LA (2013) The Tissint Martian meteorite as evidence for the largest impact excavation. Nat Commun 4:1404

Beswick AE, Carmichael ISE (1978) Constrains on mantle source compositions imposed by phosphorous and the rare earth elements. Contrib Mineral Petrol 67:317–330

Boonsue S, Spray J (2012) Shock-induced phase transformations in melt pockets within Martian meteorite NWA 4468. Spectrosc Lett 45:127–134

Dégi J, Abart R, Török K (2010) Symplectite formation during decompression induced garnet breakdown in lower crustal mafic granulite xenoliths: mechanisms and rates. Contrib Mineral Petrol 159:293–314

Dickinson JE, Hess PC (1983) Role of whitlockite and apatite in lunar felsite. Lunar Planet Sci 14:158–159

Fleet ME, Pan Y (1994) Site preference of Nd in fluorapatite [$Ca_{10}(PO_4)_6F_2$]. J Solid State Chem 112:78–81

Fleet ME, Pan Y (1995) Site preference of rare earth elements in fluorapatite. Am Mineral 80:329–335

Gaspar M, Knaack C, Meinert LD, Moretti R (2008) REE in skarn systems: a LA-ICP-MS study of garnets from the Crown Jewel gold deposit. Geochim Cosmochim Acta 72:185–205

Griffin WL, Åmli R, Heier KS (1972) Whitlockite and apatite from lunar rock 14310 and from ÖdegÅrden, Norway. Earth Planet Sci Lett 15:53–68

Hu J, Sharp TG (2016) High-pressure phases in shock-induced melt of the unique highly shocked LL6 chondrite Northwest Africa 757. Meteorit Planet Sci 51:1353–1369

Hughes JM, Cameron M (1991) Rare-earth-element ordering and structural variations in natural rare-earth-bearing apatites. Am Mineral 76:1165–1173

Jolliff BL, Haskin LA, Colson RO, Wadhwa M (1993) Partitioning in REE-saturating minerals: theory, experiment, and modeling of whitlockite, apatite, and evolution of lunar residual magmas. Geochim Cosmochim Acta 57:4069–4094

Jolliff BL, Hughes JM, Freeman JJ, Zeigler RA (2006) Crystal chemistry of lunar merrillite and comparison to other meteoritic and planetary suites of whitlockite and merrillite. Am Mineral 91:1583–1595

Konzett J, Frost DJ (2009) The high *P–T* stability of hydroxyl-apatite in natural and simplified MORB—an experimental study to 15 GPa with implications for transport and storage of phosphorus and halogens in subduction zones. J Petrol 50:2043–2062

Konzett J, Rhede D, Frost DJ (2012) The high PT stability of apatite and Cl partitioning between apatite and hydrous potassic phases in peridotite: an experimental study to 19 GPa with implications for the transport of P, Cl and K in the upper mantle. Contrib Mineral Petrol 163:277–296

Litasov KD, Podgornykh NM (2017) Raman spectroscopy of various phosphate minerals and occurrence of tuite in the Elga IIE iron meteorite. J Raman Spectrosc 48:1518–1527

Miyahara M, El Goresy A, Ohtani E, Kimura M, Ozawa S, Nagase T, Nishijima M (2009) Fractional crystallization of olivine melt inclusion in shock-induced chondritic melt vein. Phys Earth Planet Inter 177:116–121

Murayama JK, Nakai S, Kato M, Kumazawa M (1986) A dense polymorph of $Ca_3(PO_4)_2$: a high pressure phase of apatite decomposition and its geochemical significance. Phys Earth Planet Inter 44:293–303

Nash WP (1984) Phosphate minerals in terrestrial igneous and metamorphic rocks. In: Nriagu JO, Moore PB (eds) Phosphate minerals. Springer, Berlin, pp 215–241

Pan Y, Fleet ME (2002) Compositions of the apatite-group minerals: substitution mechanisms and controlling factors. Rev Mineral Geochem 48:13–49

Puchelt H, Emmermann R (1976) Bearing of rare earth patterns of apatites from igneous and metamorphic rocks. Earth Planet Sci Lett 31:279–286

Python M, Ishisa Y, Ceuleneer G, Arai S (2007) Trace element heterogeneity in hydrothermal diopside: evidence for Ti depletion and Sr–Eu-LREE enrichment during hydrothermal metamorphism of mantle harzburgite. J Mineral Petrol Sci 102:143–149

Santosh M, Rajesh VJ, Tsunogae T, Arai S (2010) Diopsidites from a Neoproterozoic–Cambrian suture in southern India. Geol Mag 147:777–788

Sheldrick GM (2015a) SHELXT—integrated space-group and crystal structure determination. Acta Crystallogr A71:3–8

Sheldrick GM (2015b) Crystal structure refinement with SHELX. Acta Crystallogr C71:3–8

Skelton R, Walker AM (2017) Ab initio crystal structure and elasticity of tuite, γ-$Ca_3(PO_4)_2$, with implications for trace element partitioning in the lower mantle. Contrib Mineral Petrol 172:87

Stöffler D, Ryder G, Ivanov BA, Artemieva NA, Cintala MJ, Grieve RAF (2006) Cratering history and lunar chronology. Rev Min Geochem 60:519–596

Sugiyama K, Tokonami M (1987) Structure and crystal chemistry of a dense polymorph of tricalcium phosphate $Ca_3(PO_4)_2$: a host to accommodate large lithophile elements in the Earth's mantle. Phys Chem Miner 15:125–130

Thompson RM, Xie X, Zhai S, Downs RT, Yang H (2013) A comparison of the $Ca_3(PO_4)_2$ and $CaSiO_3$ systems, with a new structure refinement of tuite synthesized at 15 GPa and 1300 °C. Am Mineral 98:1585–1592

Xie X, Minitti ME, Chen M, Mao HK, Wang D, Shu J, Fei Y (2002) Natural high-pressure polymorph of merrillite in the shock vein of the Suizhou meteorite. Geochim Cosmochim Acta 66:2439–2444

Xie X, Minitti ME, Chen M, Mao HK, Wang D, Shu J, Fei Y (2003) Tuite, γ-$Ca_3(PO_4)_2$: a new mineral from the Suizhou L6 chondrite. Eur J Mineral 15:1001–1005

Xie X, Zhai S, Chen M, Yang H (2013) Tuite, γ-$Ca_3(PO_4)_2$, formed from chlorapatite decomposition in the shock vein of the Suizhou L6 chondrite. Meteorit Planet Sci 48:1515–1523

Xie X, Yang H, Gu X, Downs RT (2015) Chemical composition and crystal structure of merrillite from the Suizhou meteorite. Am Mineral 100:2753–2756

Xie X, Gu X, Chen M (2016) An occurrence of tuite, γ-$Ca_3(PO_4)_2$, partly transformed from Ca-phosphates in the Suizhou meteorite. Meteorit Planet Sci 51:195–202

Xue X, Zhai S, Kanzaki M (2009) Si-Al distribution in high-pressure $CaAl_4Si_2O_{11}$ phase: a ^{29}Si and ^{27}Al NMR study. Am Mineral 94:1739–1742

Xue W, Zhai S, Zheng H (2012) Synthesis and photoluminescence properties of Eu^{3+}-doped γ-$Ca_3(PO_4)_2$. Mater Chem Phys 133:324–327

Xue W, Zhai S, Xu S (2015) Photoluminescence properties of γ-$Ca_3(PO_4)_2$:Sm^{3+} prepared under high-pressure and high-temperature conditions. Opt Mater 45:219–233

Zhai S, Kanzaki M, Katsura T, Ito E (2010a) Synthesis and characterization of strontium-calcium γ-$Ca_{3-x}Sr_x(PO_4)_2$ ($0 \le x \le 2$). Mater Chem Phys 120:348–350

Zhai S, Wu X, Ito E (2010b) High-pressure Raman spectra of tuite, γ-$Ca_3(PO_4)_2$. J Raman Spectrosc 41:1011–1013

Zhai S, Xue W, Lin C, Wu X, Ito E (2011) Raman spectra and X-ray diffraction of tuite at various temperatures. Phys Chem Miner 38:639–646

Zhai S, Yamazaki D, Xue W, Ye L, Xu C, Shan S, Ito E, Yoneda A, Yoshino T, Guo X, Shimojuku A, Tsujino N, Funakoshi K (2013) P–V–T relations of γ-$Ca_3(PO_4)_2$ tuite determined by in situ X-ray diffraction in a large-volume high-pressure apparatus. Am Mineral 98:1811–1816

Zhai S, Xue W, Yamazaki D, Ma F (2014) Trace element compositions in tuite decomposed from natural apatite in high-pressure and high-temperature experiments. Sci China: Earth Sci 57:2922–2927

Zhang RY, Liou JG, Zheng JP, Griffin WL, Yang YH, Jahn BM (2009) Petrogenesis of eclogites enclosed in mantle-derived peridotites from the Sulu UHP terrane: constraints from trace elements in minerals and Hf isotopes in zircon. Lithos 109:176–192

Zheng JP, Zhang RY, Griffin WL, Liou JG, O'Reilly SY (2005) Heterogeneous and metasomatized mantle recorded by trace elements in minerals of the Donghai garnet peridotites, Sulu UHP terrane, China. Chem Geol 221:243–259